THE JOURNAL OF PHYSICAL CHEMISTRY C

Article

pubs.acs.org/JPCC

Image Potential State Influence on Charge Exchange in Li^+–Metal Surface Collisions

Fernando J. Bonetto,*[,†,‡] Evelina A. García,[†] César González,[§] and Edith C. Goldberg[†,‡]

[†]Instituto de Física del Litoral (CONICET-UNL), Güemes 3450, S3000GLN Santa Fe, Argentina

[‡]Departamento Ingeniería Materiales, Facultad de Ingeniería Química (UNL), Santiago del Estero 2829, S3000AOM Santa Fe, Argentina

[§]Departamento de Física, Universidad de Oviedo, C/Calvo Sotelo s/n, ES-33006 Oviedo, Spain

Supporting Information

ABSTRACT: The energy dependence of the neutral fraction of ions scattered by metal surfaces is observed to be affected by the presence of energy gaps and surface states in their surface band structure. The effect is more dramatic when the ion energy level remains close to the surface Fermi level of the surface, as it occurs in the scattering of Li positive ions by Cu and noble metal surfaces. We have incorporated the interaction of the ion state with the bulk- and surface-like states within an extended Anderson model and by using an ab initio calculation of the Hamiltonian terms. In this form we found that the increase of the neutral fraction at low projectile energies is explained solely by the presence of energy gaps in the case of Cu(111), while the bonding interaction with the first image potential state is also important in the Cu(100), Ag(100), and Ag(111) surfaces.

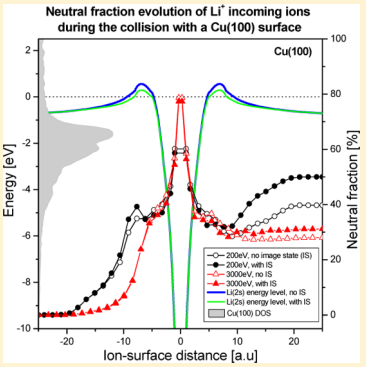

1. INTRODUCTION

Charge exchange between a projectile atom and a target surface during a nonequilibrium collision process constitutes a topic of relevance for broad areas of basic and applied research. The tunnelling of resonant electrons is essential to explain charge transfer between alkali metal ions and metal surfaces. There is abundant theoretical and experimental literature exploring these systems, but the mechanisms that control the charge exchange between them are not yet fully understood.[1−25]

When working with charge exchange during a scattering process, i.e., electronic transfer to and from a target surface to a colliding ion moving in front of it, it is important to consider that the projectile electronic energy levels are shifted and broaden with respect to the energy level at large distances. This effect is mainly due to the interaction of the projectile states with the conduction band and with the inner states of the target.[26,27]

Metallic target surfaces have work functions typically ranging from 4 to 5.5 eV. The low ionization potential of Li^+ ions (5.39 eV), comparable to metallic work functions, makes it a very attractive projectile choice for a charge exchange analysis during a collision process.[4,5,8,10,12,18−22,24,28−31]

In our previous study on this topic,[24] measurements of neutral fractions of Li^+ ions scattered by Cu(111) and Cu(100) surfaces were satisfactorily explained by applying the bond-pair model and considering an extraordinarily large number of surface atoms. However, our theoretical predictions mostly failed in explaining the large neutral fraction observed at low energies in Cu(100) and at large energies in Cu(111).

In an attempt to describe these behaviors and to fully understand the underlying charge transfer mechanisms, in the present study we investigate the inclusion of the first image potential state in Cu(100). The most relevant features of this state, such as its dispersion relation and its extension up to the borders of the surface conduction band, were considered. To complete our research, we extend the study to Ag(100) and Ag(111). It is relevant to mention that the image potential states become important only for those metal surfaces where they remain within the band gap. Otherwise, its lifetime is extremely short when compared to the time scale of a typical charge transfer experiment.[32]

Surface states can be classified according to their charge density localization relative to the surface atomic layer into intrinsic surface states and image potential states. The intrinsic surface states, those derived from the crystal potential termination at the vacuum interface,[33,34] are mainly localized at the surface atomic layer. The image potential states, derived from the long-range image potential experienced by an electron outside the surface, are mostly localized in the vacuum region of metal surfaces (beyond the image plane position z_{im}).[35−38]The binding energies of the image potential states have been measured by inverse photoemission (IPE),[36,37,39−41] two-photon photoemission (2PPE),[42−50] and time-resolved two-photon photoemission (TR2PPE)[47,51−53] techniques.

Received: November 27, 2013
Revised: March 17, 2014

   dx.doi.org/10.1021/jp4116673 | J. Phys. Chem. C XXXX, XXX, XXX−XXX

Intrinsic line widths of image potential states associated with electron−hole pair excitations have also been measured by means of 2PPE[45,46,50] and TR2PP.[47,52−54] The TR2PPE measurements have given 40−50 fs for the first image potential state on Cu(100) and Ag(100),[47,49] 15−18 fs for Cu(111),[49,53] and 30 fs for Ag(111).[55]

The influence of the image potential states on the charge exchange in low-energy ion−metallic surface collisions has been barely treated in the past. Borisov et al.[13] include the intrinsic surface state in the wave packet approximation method to calculate the resonant charge transfer in ion−metal surface collisions, with special emphasis on the H^-/Cu(111) system. Nevertheless, in most of the theoretical models used to describe the experimental neutralization rates, the image potential is only intended to shift the projectile energy level at large distances.[20,22,24,29,31] In contrast, here we consider the image potential state as another state of the surface that interacts with the active state of the projectile, within the Anderson model approach. The corresponding density of states and image potential state energy dispersion with the wave vector parallel to the metallic surface are also included.

It is pertinent to state that we use a local density approximation for calculating the electronic structure of the metal surface which satisfactorily describes the intrinsic surface states but not the image potential surface states. The calculation of the image potential states is performed by matching a long-range image potential onto the self-consistent crystal potential by following the proposal of Chulkov et al.[56]

In the present paper we show that the image potential state influence on charge exchange processes involving low-energy colliding Li^+ ions on metallic surfaces is by no means negligible. Furthermore, we find that its effect becomes more significant at lower projectile kinetic energies. The role played by the image potential state in charge transfer strongly depends on two main factors: (i) how strong is the bonding interaction with the projectile energy level and (ii) how extended is the image potential state within the surface band gap of the metallic surface.

2. THEORY

2.1. Interaction Model. The atom−surface interaction is described by the extended Anderson Hamiltonian given by the expression

$$H = \sum_{\vec{k},\sigma} \varepsilon_{\vec{k}} \hat{n}_{\vec{k}\sigma} + H_{\text{atom}} + H_{\text{atom-surface}} \tag{2.1}$$

The first term in eq 2.1 refers to the solid states of energy $\varepsilon_{\vec{k}}$ and occupation number $\hat{n}_{\vec{k}\sigma}$ per spin projection σ. The second term is related with the atom electronic configurations considered as the most probable ones in the charge exchange process, and finally the last term is the interaction between these electronic configurations and the band states of the solid surface.

In this work, we consider only the resonant neutralization to the ground state of the Li atom, and then the H_{atom} in the case of neglecting the spin variable (spinless approximation) is given by the expression

$$H_{\text{atom}} = \varepsilon_I \hat{n}_a \tag{2.2}$$

Within the *bond-pair* model used for describing the atom−surface interaction,[57] the difference between total energies $E(1s^2\ 2s) - E(1s^2)$ gives asymptotically the Li ionization energy; by considering only the contributions of the short-range interaction terms it results to be

$$\tilde{\varepsilon}_I = E(1s^2 2s) - E(1s^2) = \varepsilon_0 - \sum_{\vec{R}_s} V_{2s,2s}^{Z_s,\vec{R}_s} + \sum_{i,\vec{R}_s} (2\tilde{J}_{2s,i\vec{R}_s} - \tilde{J}^X_{2s,i\vec{R}_s})\langle n_i\rangle - \sum_{i,\vec{R}_s} S_{2s,i\vec{R}_s} V^{\text{dim}}_{2s,i\vec{R}_s} + \frac{1}{4}\sum_{i,R_s} S^2_{2s,i\vec{R}_s} \Delta E_{2s,i\vec{R}_s} \tag{2.3}$$

In eq 2.3 the index i denotes the type of orbital (s, p, d, ...) and $\vec{R}_s$ the position of the atoms in the solid, while 2s indicates the active state in the projectile atom. The $\varepsilon_0 - \sum_{\vec{R}_s} V_{2s,2s}^{Z_s,\vec{R}_s}$ term accounts for the one-electron contributions (kinetic energy and electron−nuclei interactions); $\tilde{J}_{2s,i\vec{R}_s}, \tilde{J}^X_{2s,i\vec{R}_s}$ are the direct and exchange Coulomb integrals calculated up to a second-order expansion in the overlap $S_{2s,i\vec{R}_s}$ of the symmetric orthogonal atomic basis set. The average occupations $\langle n_i\rangle$ of the atoms in the solid are the nonperturbed ones obtained from the local surface density of states. The $\Delta E_{2s,i\vec{R}_s}$ term corresponds to the difference between the projectile atom and surface atom energy terms, and $V^{\text{dim}}_{2s,i\vec{R}_s}$ is the off-diagonal term that also includes the two-electron contributions to the hopping within a mean-field approximation. The superindex dim indicates that it is calculated within the orthogonal basis set for the corresponding dimer composed by the projectile atom and one of the solids at the position $\vec{R}_s$. The total energies are calculated without allowing charge exchange between the atom and surface, the Li energy level variation being caused by overlap and mean-field electrostatic interactions.

The effect of the long-range interactions is introduced by considering the image potential defining the behavior for large normal distances (z) to the surface ($z > z_a$)[57,58]

$$\varepsilon_I(R) = \begin{cases} \tilde{\varepsilon}_I(R) + V_{\text{im}}(z_a) \text{ for } z \le z_a \\ \tilde{\varepsilon}_I(R) + V_{\text{im}}(z) \text{ for } z > z_a \end{cases} \tag{2.4}$$

where

$$V_{\text{im}}(z) = \frac{1}{4(z - z_{\text{im}})}$$

and z_{im} is the image plane distance from the first surface layer of atoms.

Consistently with this picture, the $H_{\text{atom-surface}}$ is

$$H_{\text{atom-surface}} = \sum_{\vec{k}} [V_{\vec{k},2s}\hat{c}^+_{\vec{k}}\hat{c}_a + hc] \tag{2.5}$$

The wave vectors $\vec{k} = (\vec{k}_{//}, k_z)$, which classify the bulk and surface-like states $\psi_{\vec{k}}(\vec{r})$ of a solid with surface, are only Bloch vectors in the parallel direction to the surface ($\vec{k}_{//}$). The coupling term $V_{\vec{k},2s}$ in the case of bulk and intrinsic surface[59] states is calculated as usual according to the expansion of $\psi_{\vec{k}}(\vec{r})$ in atomic orbitals centered on the surface atoms ($\phi_i(\vec{r} - \vec{R}_s)$)

$$V_{\vec{k},2s} = \sum_{i,\vec{R}_s} c^{\vec{k}}_{i,\vec{R}_s} V^{\text{dim}}_{2s,i\vec{R}_s} \tag{2.6}$$

The coefficients $c^{\vec{k}}_{i,\vec{R}_s}$ determine the density matrix elements $\rho_{i,j,\vec{R}_s,\vec{R}_{s'}}(\varepsilon)$ of the solid through the expression

dx.doi.org/10.1021/jp4116673 | J. Phys. Chem. C XXXX, XXX, XXX−XXX

$$\rho_{i,j,\vec{R}_s,\vec{R}_{s'}}(\varepsilon) = \sum_{\vec{k}} c^{\vec{k}*}_{i,\vec{R}_s} c^{\vec{k}}_{j,\vec{R}_{s'}} \delta(\varepsilon - \varepsilon_{\vec{k}}) \tag{2.7}$$

The density matrix $\rho_{i,j,\vec{R}_s,\vec{R}_{s'}}(\varepsilon)$ is calculated by using the Local Density Approximation (LDA).[60,61] As the LDA does not reproduce the correct asymptotic behavior of the image potential in the vacuum, the calculation of the image potential states is performed by matching a long-range image potential onto the self-consistent crystal potential. By following the proposal of Chulkov et al.,[56] the resulting potential V_{metal} is constant in the x, y plane and varies in the z direction (see the Supporting Information). The coupling term in the case of image potential state is calculated as

$$V^{\text{image}}_{\vec{k},2s} = \langle \psi_{\vec{k}} | T + V_{\text{atom}} + V_{\text{metal}} | \psi_a \rangle \tag{2.8}$$

where T is the kinetic energy term and V_{atom} (V_{metal}) is the potential energy due to the atom (surface). Taking into account that $(T + V_{\text{atom}})\psi_a \approx \varepsilon_a \psi_a$ and that $\psi_{\vec{k}}$ and ψ_a are orthonormalized (see Supporting Information for details), eq 2.8 is approximately given by the expression

$$V^{\text{image}}_{\vec{k}_{//},2s}(z) = \langle \psi_{\vec{k}} | V_{\text{metal}} | \psi_a \rangle \tag{2.9}$$

The details of the calculation are given in the Supporting Information for each metal surface of interest.

It is important to notice that the inner bands of the surface (3s, $3p_x$, $3p_y$, and $3p_z$ for Cu surfaces and 4s, $4p_x$, $4p_y$, and $4p_z$ for Ag surfaces) are straightforwardly included in our calculation by considering them as zero-width bands.

2.2. Time-Dependent Calculation of the Atom Charge State Probabilities. We use the following Green functions to solve the time evolution introduced by the time dependence of the projectile position with respect to the surface ($\vec{R} = \vec{R}(t)$)

$$G_a(t, t') = i\Theta(t' - t)\langle \Phi_0 | \{\hat{c}_a^+(t'), \hat{c}_a(t)\} | \Phi_0 \rangle$$

$$F_a(t, t') = i\langle \Phi_0 | [\hat{c}_a^+(t'), \hat{c}_a(t)] | \Phi_0 \rangle \tag{2.10}$$

Φ_0 being the wave function that describes the interacting system in the Heisenberg scheme. The neutralization probability is given in this case by the average occupation of the atomic state $\langle \hat{n}_a(t) \rangle$ which is obtained from $F_a(t,t')$ at equal times $t = t'$

$$F_a(t, t) = i\langle 1 - 2\hat{n}_a(t) \rangle$$

The Green functions are calculated by using the method of equations of motion (EOM) which leads to the differential expressions

$$i\frac{d}{dt}G_a(t, t') = \delta(t - t') + \varepsilon_I G_\sigma(t, t') + \int_t^{t'} d\tau \Sigma_a^A(t, \tau) G_a(\tau, t') \tag{2.11}$$

$$i\frac{d}{dt}F_a(t, t') = \varepsilon_I F_a(t, t') + \int_{t_0}^{t} d\tau \Sigma_a^R(t, \tau) F_a(\tau, t') + \int_{t_0}^{t'} d\tau \Omega_a(t, \tau) G_a(\tau, t')$$

The self-energies determining the motion equations of these Green functions read

$$\Sigma_a^A(t, \tau) = i\Theta(\tau - t) \sum_{\vec{k}} V_{2s,\vec{k}}(t) V_{\vec{k},2s}(\tau) e^{i\varepsilon_{\vec{k}}(\tau - t)} = \Sigma_a^{R*}(\tau, t) \tag{2.12}$$

$$\Omega_a(t, \tau) = i \sum_{\vec{k}} V_{2s,\vec{k}}(t) V_{\vec{k},2s}(\tau) e^{i\varepsilon_{\vec{k}}(\tau - t)} (2\langle \vec{n}_{\vec{k}} \rangle - 1) \tag{2.13}$$

In eq 2.13 $\langle \vec{n}_{\vec{k}} \rangle$ is given by the Fermi function $1/[1 + e^{(\varepsilon_{\vec{k}} - \varepsilon_F)/k_B T}]$ (ε_F is the Fermi energy and T the temperature).

The contributions to the self-energies 2.12 and 2.13 coming from the bulk and intrinsic surface states can be separated from those coming from the image potential states. In the first case, by using eqs 2.6 and 2.7, we have

$$\Sigma_a^{A(b+SS)}(t, \tau) = i\Theta(\tau - t) \sum_{i,j,\vec{R}_s,\vec{R}_{s'}} V^*_{i\vec{R}_s,2s}(t) V_{j\vec{R}_{s'},2s}(\tau) \int_{-\infty}^{\infty} d\varepsilon \rho_{i,j,\vec{R}_s,\vec{R}_{s'}}(\varepsilon) e^{i\varepsilon(\tau - t)} \tag{2.14}$$

The contribution from the image potential states can be written as

$$\Sigma_a^{A(IS)}(t, \tau) = i\Theta(\tau - t) \sum_{\vec{k}} V^{\text{image}}_{2s,\vec{k}}(t) V^{\text{image}}_{\vec{k},2s}(\tau) e^{i\varepsilon_{\vec{k}}(\tau - t)} = i\Theta(\tau - t) \int d\varepsilon \rho_{IS}(\varepsilon) V^{\text{image}}_{2s,\varepsilon}(t) V^{\text{image}}_{\varepsilon,2s}(\tau) e^{i\varepsilon(\tau - t)} \tag{2.15}$$

The density of states $\rho_{IS}(\varepsilon)$ takes into account the energy dispersion in $\vec{k}_{//}$ of the surface image potential states.

2.3. Shift and Width of the Ion Energy Level Due to the Adiabatic Interaction. The shift and the width of the energy level of the ion interacting adiabatically with the metal surface can be extracted from the Anderson hybridization function given by the Fourier transform of the self-energy $\Sigma_a^A(t,\tau)$ (eq 2.12)

$$\Sigma_a^A(\omega) = \lim_{\eta \to 0} \sum_{\vec{k}} \frac{|V_{2s,\vec{k}}|^2}{\omega - \varepsilon_{\vec{k}} - i\eta} \tag{2.16}$$

The atom energy level shift corresponds to the real part of $\Sigma_a^A(\omega)$, $\bar{\varepsilon}_I$ being defined as

$$\bar{\varepsilon}_I(\vec{R}) = \varepsilon_I + \text{Re}\, \Sigma_a^A(\varepsilon_I) \tag{2.17}$$

and the level width Γ is defined as twice the imaginary part of 2.16

$$\Gamma(\vec{R}) = 2\, \text{Im}\, \Sigma_a^A(\bar{\varepsilon}_I) \tag{2.18}$$

Both the shift and the width of the atom energy level are functions of the atom position $\vec{R}$.

3. RESULTS AND DISCUSSION

3.1. Convergence of Neutralization with the Number of Surface Atoms Considered. To complete the study reported in ref 24, in Figure 1 we show the convergence of the calculation with the number of surface atoms considered for the Li−Cu(111) and Li−Cu(100) systems. In this figure we present the results of the calculation by increasing the number of surface atoms up to first, second, third, fourth, and fifth nearest neighbors.

dx.doi.org/10.1021/jp4116673 | J. Phys. Chem. C XXXX, XXX, XXX−XXX

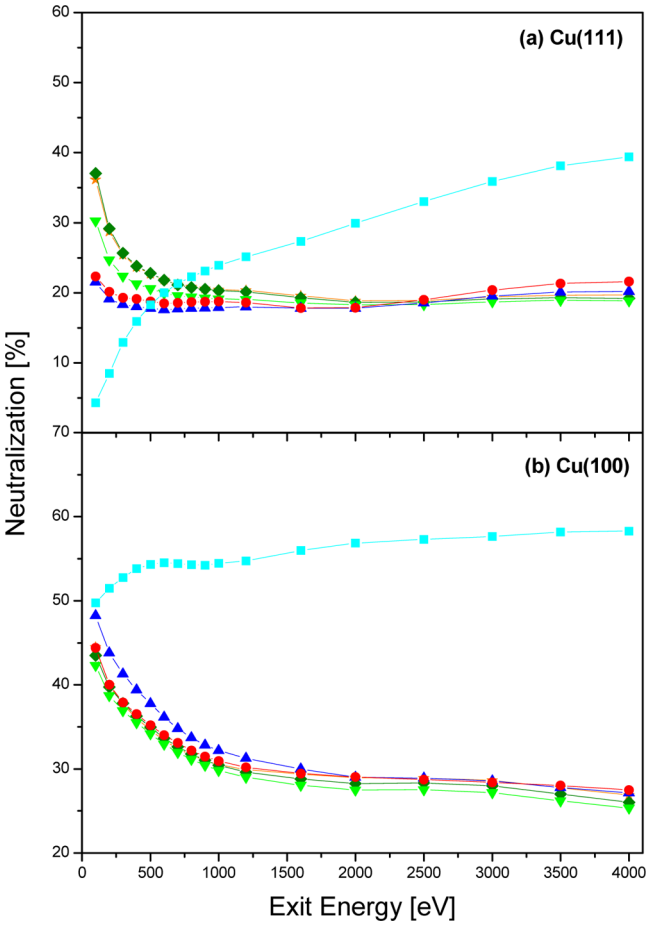

Figure 1. Neutralization as a function of the exit projectile energy for scatter atom (turquoise square); first (red circle); second (blue up triangle); third (green down triangle); fourth (green diamond); and fifth (yellow star) nearest neighbors. (a) Cu(111) and (b) Cu(100). Convergence with the number of surface atoms considered can be clearly appreciated.

From these curves, the convergence of the calculation when up to four nearest neighbors are included is straightforward (37/34 atoms for Cu(111)/Cu(100)).

An analogous study (not shown) was performed for Ag(100) and Ag(111), arriving to similar conclusions: convergence is achieved when up to four nearest neighbors are included. This result is a consequence of the fact that both crystallographic faces analyzed ((111) and (100)) exhibit similar characteristics (same crystal structure and comparable lattice parameters) in copper and silver.

It is worth noting also that a completely different trend and absolute values are obtained when only one atom (scatter atom) and many atoms are considered. This result demonstrates how crucial the scatter neighboring atoms are and the interferences between them to explain the experimental neutralization behavior, particularly in the low-energy regime.

3.2. Atom Energy Level and Hoppings. Equations 2.3 and 2.4 are used to calculate the Li ionization energy level, using a full electron description of the Li−Cu and Li−Ag interacting systems. The image plane position z_{im} is assumed to be half of the interlayer distance: 1.71 au, 1.97 au, 2.27 au, and 1.93 au for Cu(100), Cu(111), Ag(111), and Ag(100) respectively.[62]

The hopping with bulk and intrinsic surface states (eq 2.6) is calculated in terms of the atom−atom hopping integrals $V^{dim}_{2s,i\vec{R}_s}$, provided by the bond-pair model.[57] They are also symmetrically orthogonalized within the set of substrate atoms considered in the calculation of $\rho_{i,j,\vec{R}_s,\vec{R}_{s'}}(\varepsilon)$ by using the FIREBALL code.[60,61] This code is based on a density functional theory within a local density approximation that employs a localized numeric-like orbital basis set.

The energy level as a function of the distance to the surface (z) is depicted in Figure 2 for the Li atom in front of both Cu and Ag surfaces (the zero energy corresponds to the Fermi level). It is also shown in this figure the local density of states projected on one surface atom, calculated as

$$\rho_{\vec{R}_s}(\varepsilon) = \sum_{i,j=3d,4s,4p} \sum_{\vec{k}} c^{\vec{k}}_{i,\vec{R}_s} c^{\vec{k}}_{j,\vec{R}_s} \delta(\varepsilon - \varepsilon_{\vec{k}})$$

The distance dependence of the projectile 2s state was calculated by considering in eq 2.3 the interaction with (i) only the scatter atom on the surface at R_s = (0,0,0) and (ii) the scatter atom and up to its fourth nearest neighbors. Although not significant in all the cases studied, a downshift of the level is observed when a high number of surface atoms are considered in the calculation. It is important to notice that when the projectile is leaving the surface ($z > 0$) the ion energy level intersects two times the surface Fermi level. The second crossing point (here, the projectile energy level crosses from above to below the Fermi level) takes place at relatively short distances ($z < 15$ au in all cases) where the interaction is still operative since the energy width is still significant. This fact is essential to explain the typical increase in neutralization observed at low exit energies of Li projectiles interacting with metallic surfaces.[24]

The atom−atom hopping integrals $V^{dim}_{2s,i\vec{R}_s}$ by considering and not considering the orthogonalization effects are compared in Figure 3.

On copper surfaces, relevant differences between atomic and orthogonal hoppings can only be noticed in interactions of the projectile active state with 4s and 4p states of the scatter surface atoms. No visible differences are observed in silver surfaces. Despite these small changes, a cumulative effect due to the large number of surface atoms considered can lead to appreciable differences in neutralization rates. Therefore, orthogonalization must be performed to ensure a good description of the interaction between the projectile and the surface atoms.

The hopping with the image potential state $V^{image}_{k//,2s}(z)$ calculated as it is detailed in the Supporting Information is shown in Figure 4 as a function of the normal distance to the surface (z) and for $\vec{k}_{//} = 0$.

Of particular importance are the extension (up to about 25 au) and the position of the minimum (between 5 and 10 au) of the hoppings when considering nonorthogonal states, shown in Figure 4. These features lead to an effect on the neutralization rates not so dependent on the projectile energy since the region of major influence of the hopping covers the different effective distances of charge exchange which vary from relatively small values for rapid projectiles to large values for slow projectiles. In general, less localized hopping interactions conduct to less energy-dependent neutralization rates. The hoppings calculated by considering orthogonalized states are substantially more localized, thus a higher dependence with the projectile incoming energy is expected in this case.

dx.doi.org/10.1021/jp4116673 | J. Phys. Chem. C XXXX, XXX, XXX−XXX

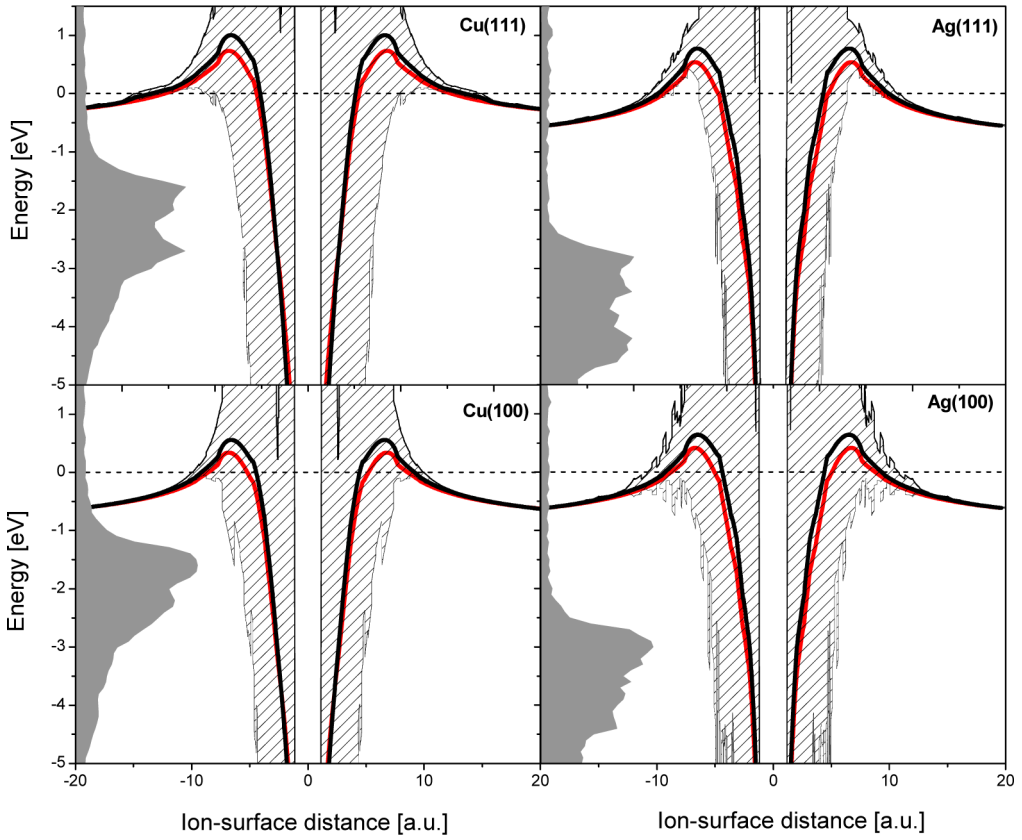

Figure 2. Distance dependence of the Li ionization energy level: (a) Cu(111), (b) Cu(100), (c) Ag(111), and (d) Ag(100) when the interaction with only the scatter atom is considered (red line) and when up to four nearest neighbors are included (black line). The shadowed area corresponds to the Cu and Ag surface LDOS. The dotted line indicates the Fermi energy level, and the striped area corresponds to the energy level width.

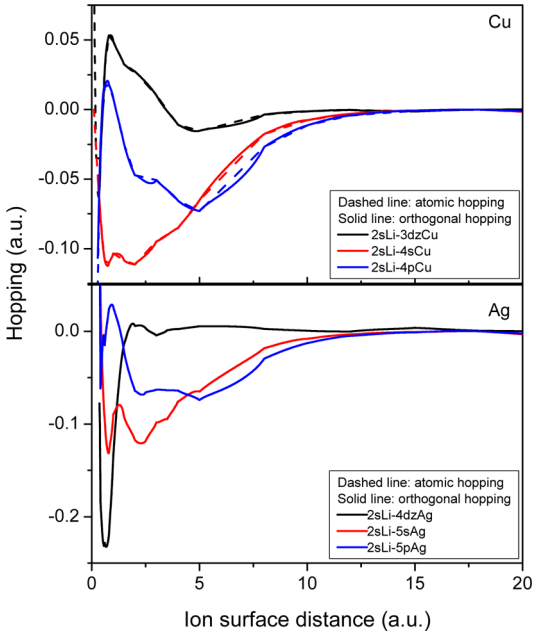

Figure 3. Orthogonalized (solid line) and nonorthogonalized (dashed line) coupling terms between the projectile ion and the scatter atom as a function of ion−surface distance for (a) 2sLi−3d_zCu (black); 2sLi−4sCu (red); 2sLi−4p_zCu (blue) and (b) 2sLi−4d_zAg (black); 2sLi−5sAg (red); 2sLi−5p_zAg (blue).

3.3. Atom Energy Level Width and Shift Due to the Adiabatic Interaction with the Image Potential State.

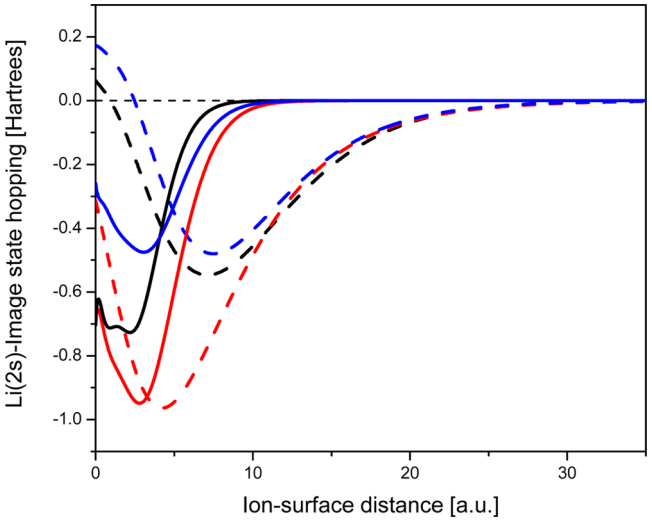

Figure 4. Dependence of the 2sLi-image potential state hopping with the normal distance to the target surface (assuming $k_{//} = 0$) for Cu(100) (black line), Ag(100) (red), and Ag(111) (blue) by considering the orthogonalization effect (solid line) and by neglecting it (dashed line).

The energy width and shift caused by the interaction with the image potential state can be appreciated in Figure 5.

From Figure 5, it is clear that only a negligible level width is introduced by the image potential state on the three surfaces analyzed when compared to level widths shown in Figure 2. On the contrary, the energy shift induced by the presence of the

dx.doi.org/10.1021/jp4116673 | J. Phys. Chem. C XXXX, XXX, XXX−XXX

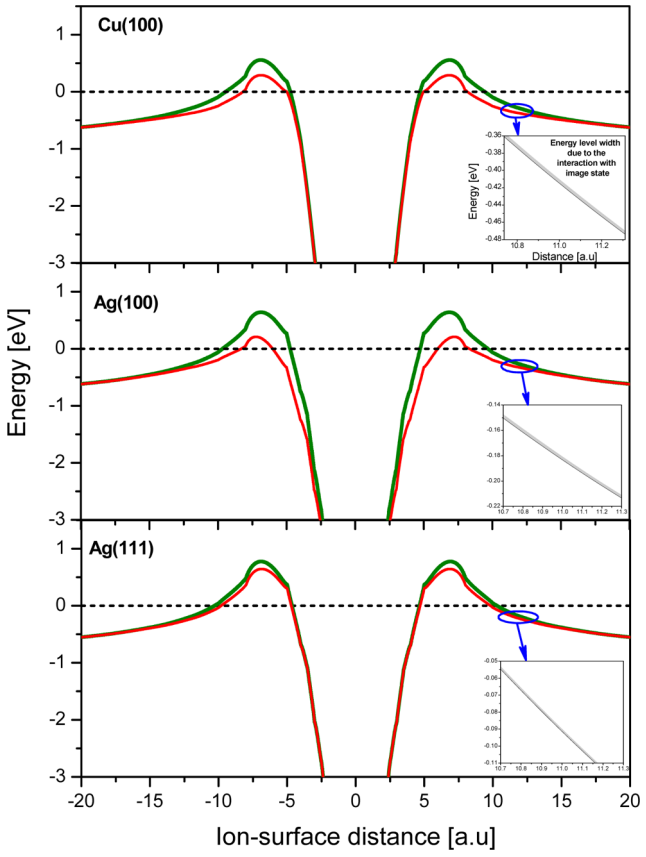

Figure 5. Energy shift as a function of ion−surface distance. The ionization Li energy level (olive line) and the Li ionization energy level shifted by the interaction with image potential state (red line) are compared. The dotted line indicates the Fermi energy level. Inset: energy level width due to the interaction with image potential state.

image potential state is by no means irrelevant. A downshift is established in all cases, but it is visibly more significant in (100) surfaces. This outcome shows consistency with eqs 2.16 and 2.17. These equations tell us: (i) stronger image-projectile state interactions correspond to larger downshifts (see Figure 4) and (ii) longer extensions of the image potential state within the surface band gap are associated also to larger downshifts (see Supporting Information for details). Similar changes are envisioned for neutralization rates.

3.4. Dynamic Collision Process: Neutralization Probability. Our theoretical calculations are performed by considering a backscattering geometry, and then it is expected to provide a good description of the measurements of refs 29 and 30 performed by using a scattering angle δ of 114° and an exit angle normal to the surface (β = 90°) and of ref 24 that corresponds to the same exit angle but with δ = 135°. Our calculations take into account the experimental setup by considering incoming and exit velocity values equal to the perpendicular components of the experimental scattering geometry.

This means that our results were obtained assuming a normal trajectory with the corresponding normal component of the incoming energy $E_{in} = E_k \sin^2 \Phi_{in}$ and an exit energy $E_{out} = KE_k$, E_k being the incoming ion kinetic energy and K the energy loss factor for the binary collision of the Li−Cu(Ag) system at a scattering angle of δ. The distance of closest approach at the different incoming energies is consistently calculated with the binary collision model from the interaction energy of the dimer Li−Cu(Ag) system. The inner band states of the metal surface (3s, 3p for Cu and 4s, 4p for Ag) were also included in the calculation. Parallel velocity effects[3,14,63] due to the outgoing motion of the projectile perpendicular to the surface are not present in this case.

The experimental and theoretical results (not considering the image potential state) are contrasted in Figure 6 for the four surfaces studied. Except for Cu(111) and Ag(100), where differences are more appreciable, a good agreement is obtained at higher energies. The neutral fraction increase experimentally observed at lower energies is not very well reproduced by the theoretical results; however, an important improvement in the general trend has been achieved when a large number of surface atoms are incorporated in the calculation.

To explore if these drawbacks of the theoretical model can be corrected, we incorporated the image potential state in our calculation model, following the procedure detailed in the Supporting Information. Results including the image potential state with orthogonal and nonorthogonal wave functions are shown in Figure 7. The calculation was performed for Li/Cu(100), Li/Ag(100), and Li/Ag(111). The system Li/Cu(111) was omitted since its image potential state is located within the conduction band, leading to a very short lifetime.

For nonorthogonal wave functions, the image potential state tends to increase the neutralization rate in the whole energy range, and as we previously have foreseen, its influence hardly depends on the projectile energy. On the Li−Cu(100) system, it sensibly improves the description of neutralization rates observed. On Li−Ag(100) the presence of the image potential state significantly improves the description at higher energies (the results obtained in this regime exactly match the experimental data). An increase in the neutralization is introduced by the image potential state at lower energies, but it is not sufficient to reproduce the experimental results.

After orthogonalization, no substantial changes are observed in the neutral fractions obtained in the low-energy range. However, when compared to experimental data, the general trend notably improves since a higher dependence on the incoming energy, mainly caused by a more localized hopping interaction, is observed.

On Li−Ag(111) the effect of the image potential state is minor, mainly due to its proximity to the border of the conduction band. However, the difference between experimental and theoretical neutralization is diminished when the image potential state is considered.

3.5. Analysis of Neutralization Evolution: Trajectories. To explore how the image potential state−Li(2s) interaction is affecting the neutralization rate, we calculated the evolution of the Li(2s) neutral fraction as the collision is produced. Results for the Li−Cu(100) system are plotted in Figure 8. Neutral fractions obtained when the image potential state is included and not are compared for two different projectile exit energies. The total DOS and the energy shift are also included in the graph to facilitate the reading and the evaluation of the neutral fraction progression as the projectile interacts with the surface. In this plot, we assume the surface positioned at z = 0, and negative/positive distances are associated with incoming/outgoing trajectories of the projectile.

At first glance we can make the following observations when the neutralizations considering and not considering the image potential state influence are compared:

(i) At the end of the incoming trajectories, both results nearly match, meaning that the differences are established at the

dx.doi.org/10.1021/jp4116673 | J. Phys. Chem. C XXXX, XXX, XXX−XXX

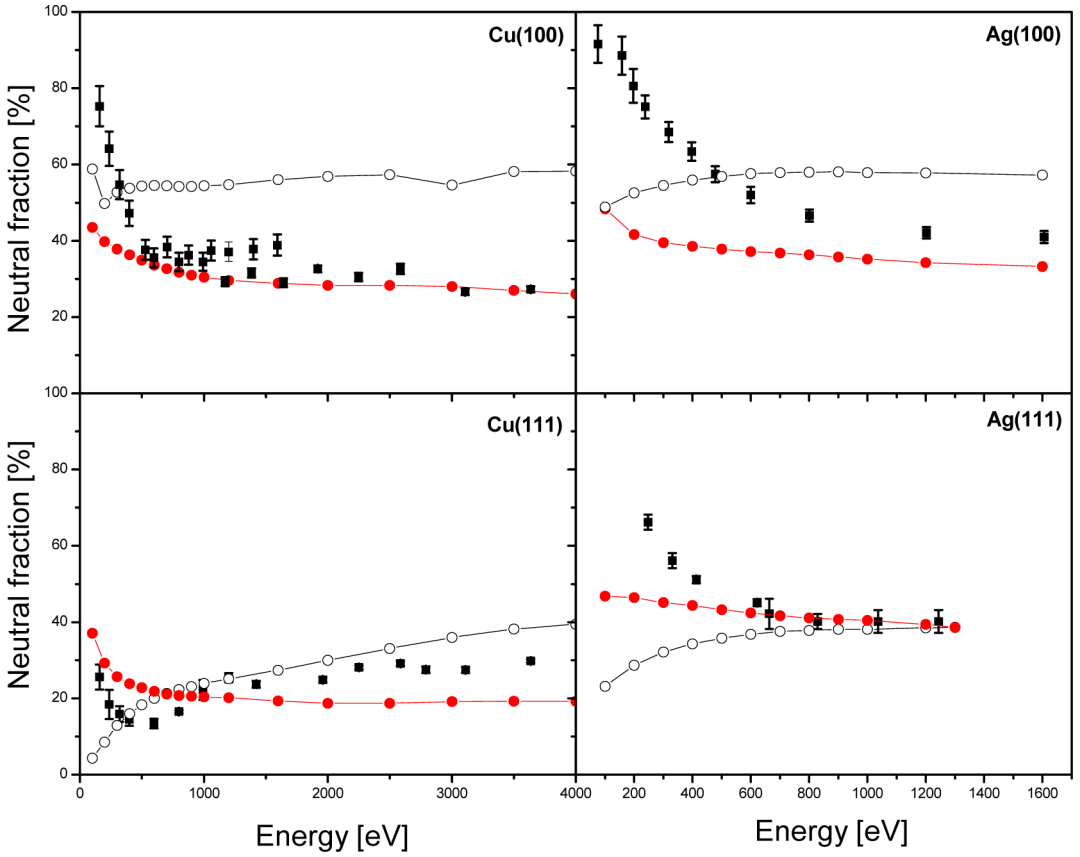

Figure 6. Neutralization as a function of the projectile exit energy (the image potential state is not considered). The experimental data (black full square) corresponding to refs 24 and 30 for Cu(100), refs 24 and 29 for Cu(111), ref 16 for Ag(100), and ref 29 for Ag(111) are contrasted with theoretical results when only the scatter atom (black open circles) and up to four nearest neighbors (red full circles) are considered.

outgoing trajectory. This result is common for both lower and larger energies.

(ii) At the outgoing trajectory, neutral fractions start to separate at an ion−surface distance of 9 au (11 au) for 200 eV (3000 eV). This result is associated with the ion energy level crossing (from above to below) the surface Fermi level. For higher projectile energies this effect starts later and is less pronounced since fast projectiles tend to "average" the details of the different characteristics of the target surface (i.e., DOS, position of the surface Fermi level relative to the projectile energy) turning high speed ion neutral fractions less sensitive to all these features.

Note that this behavior is also observed in the incoming trajectory.

(iii) The increase of neutral fractions in the whole energy range is directly linked to the downshift of the Li energy level produced by the interaction with the image potential state.

An analogous analysis can be made for the other systems; however, we decided to focus on the system where most relevant changes are produced.

With the purpose of exploring the grounds of the energy level downshift produced by the Li(2s)−image potential state interaction, we calculated (see Figure 9) the bonding interaction of Li(2s) with the image potential state assuming no dispersion on $k_{//}$ of the latter. That is, the image potential state energy value ε_{im} was assumed to be constant and equal to ε_{im} $(k = 0)$.

To perform the calculation we use the following equation

$$E_b(z) = \frac{\varepsilon_{im} + \varepsilon_I}{2} - \left(\frac{(\varepsilon_{im} - \varepsilon_I)^2}{4} + (V^{image}_{\vec{k}_{//},2s}(z))^2 \right)^{1/2}$$

where E_b is the bonding energy; ε_{im} is the energy of the image potential state; ε_I is the energy level of the Li(2s); and $V^{image}_{k//,2s}$ is the hopping interaction function depending on the ion distance z (see Figure 4).

Despite that the calculation of the bonding state only pretends to be a rough approach on how the energy level downshift is produced, it is clearly illustrating the tendency shown in Figure 5. Results displayed in Figures 4, 5, 7, and 9 show a remarkable consistency: stronger hoppings (Figure 4) are associated with larger energy downshifts (Figure 5) and larger differences between the bonding and projectile states (Figure 9). As a direct consequence, more significant changes in neutralization rates are introduced by the image potential state (Figure 7).

4. CONCLUSIONS

In this work we performed a time-dependent quantum mechanical calculation of the resonant neutralization probability to the ground state of Li^+ impinging on Cu(100), Cu(111), Ag(100), and Ag(111) for different incident energies. From the results presented above we can conclude:

(1) The calculation converges when up to four nearest neighbors are considered in the surface. The inclusion of a large number of surface atoms significantly improves the description of neutralization rates at lower energies. This fact directly

dx.doi.org/10.1021/jp4116673 | J. Phys. Chem. C XXXX, XXX, XXX−XXX

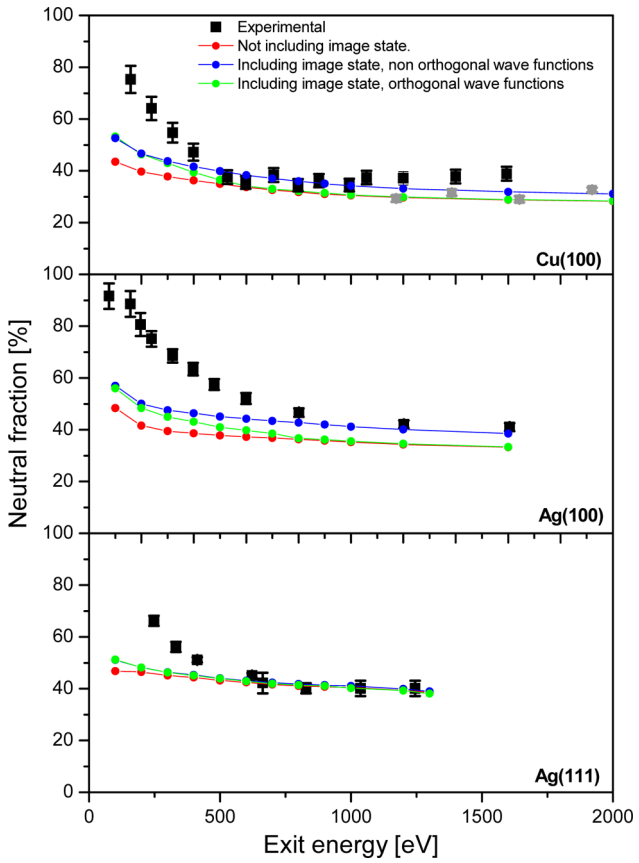

Figure 7. Neutralization as a function of the projectile exit energy. Experimental data (black and gray squares) correspond to the same references as in Figure 6. The theoretical results when the image potential state is not included and included, considering orthogonal and nonorthogonal wave functions, are compared.

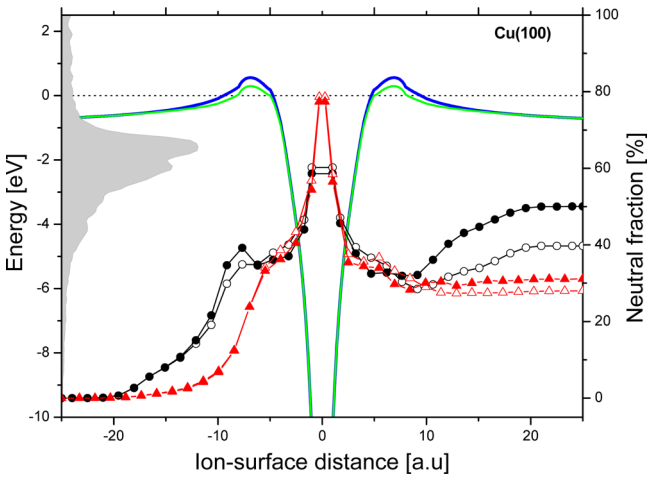

Figure 8. Normal distance dependence of the calculated neutral fraction along the trajectory for the Cu(100) face and two different projectile exit energies: without image potential state for 200 eV (open black circles) and 3000 eV (open red triangles) and with image potential state for 200 eV (full black circles) and 3000 eV (solid red triangles). Green and blue lines correspond to 2sLi variation when the image potential state is and is not included, respectively. The Cu total local DOS (shadowed area) is also shown. The dotted line indicates the surface Fermi level.

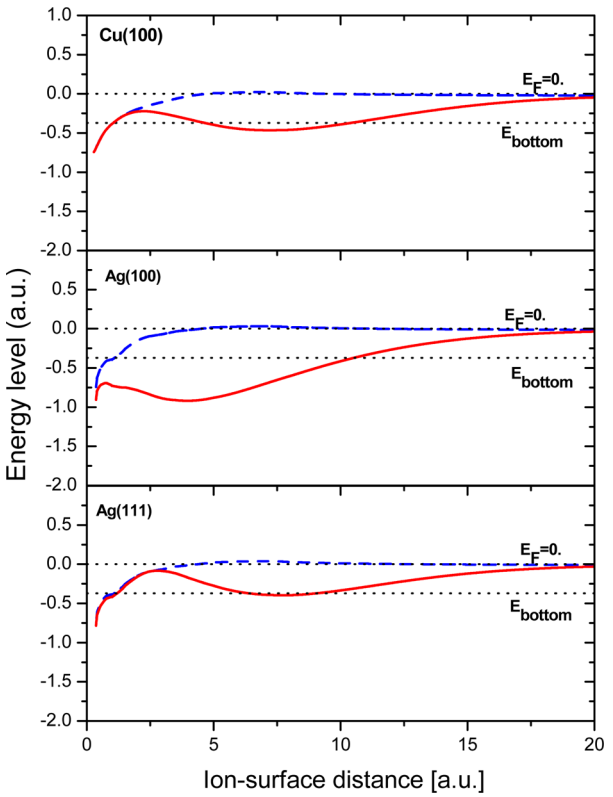

Figure 9. Bonding interaction of 2sLi with the image potential state as a function of ion−surface distance (the image potential state energy value was assumed constant, $k_{//} = 0$). Blue dashed line corresponds to the ionization Li2s energy level and the red solid line to the bonding energy level. The Fermi energy level and the energy of the bottom of the bands are also indicated (dotted line).

indicates that the fine details of the surface band structure are very important in the analyzed systems.

(2) Orthogonalization introduces minor changes in the hopping terms of both systems. However, it should be included if an accurate calculation is required.

(3) The interaction of the Li^+ active state with the surface image potential state introduces an energy width that can be neglected when compared to the total width produced by the interaction with the other states of the surface atoms. However, the energy downshift associated with a bonding interaction is significant and able to cause notable changes in the neutralization rates. The energy dispersion of the image band state has to be considered to get a better description of the charge exchange process.

(4) Neutral fractions tend to be increased because of the interaction with the image potential state in the whole range of the energies studied. This effect is slightly more pronounced at lower energies and directly associated with the downshift provoked by this interaction and to the proximity of the Li(2s) energy level to the surface Fermi level.

(5) When compared to experimental data, the introduction of image potential states clearly improves the calculation in all cases. This constitutes an evident step up in the description of charge transfer during ion−metal surface collisions. A better description of the experimental neutralizations vs energy dependence is obtained after orthogonalization of Li 2s and image state wave functions. However, no significant differences in the magnitude of neutral fractions are found.

dx.doi.org/10.1021/jp4116673 | J. Phys. Chem. C XXXX, XXX, XXX−XXX

(6) Main changes introduced by the image potential state in the neutralization rates are totally defined in the last part of the outgoing trajectory (ion−surface distance larger than 9 au).

Finally, the remaining differences between theoretical and experimental results might be attributed to (i) small errors inherent to the LDA calculation of the surface density matrix that may lead to large differences in the neutral fraction calculation or (ii) other charge state configurations of the Li atoms, such as excited and negative ion states that cannot be clearly disregarded in the interaction with the surface. These other neutralization channels are expected to be more probable in the case of the lowest work function surface, i.e., Cu(100). However, it is important to have in mind that the potential correlation effects are always difficult to predict.

■ ASSOCIATED CONTENT

Supporting Information

Additional theoretical details on adiabatic interaction with the image potential state: the hopping with the image potential state and wave functions and hopping orthogonalization. This material is available free of charge via the Internet at http://pubs.acs.org.

■ AUTHOR INFORMATION

Corresponding Author

*Tel.: +54-342-4559175. Fax: +54-342-4550944. E-mail: bonetto@santafe-conicet.gov.ar.

Notes

The authors declare no competing financial interest.

■ ACKNOWLEDGMENTS

This work was supported by ANPCyT through PICT-2007-00811, 2010-0294 CONICET through PIP-00621, and U.N.L. through CAI+D grants.

■ REFERENCES

(1) Huzinaga, S. Gaussian Type Functions for Polyatomic Systems. I. *J. Chem. Phys.* **1965**, *42*, 1293.

(2) Boers, A. L. Charge State of Low Energy Reflected Alkalis. *Nucl. Instrum. Methods Phys. Res., Sect. B* **1984**, *2*, 353−359.

(3) Los, J.; Geerlings, J. J. C. Charge Exchange in Atom-Surface Collisions. *Phys. Rep.* **1990**, *190*, 133−143.

(4) Ashwin, M. J.; Woodruff, D. P. Charge Exchange Processes in Li+ and He+ Ion Scattering from Alkali Adsorbates on Cu(110). *Surf. Sci.* **1991**, *244*, 247−258.

(5) German, K. A. H.; Weare, C. B.; Varekamp, P. R.; Andersen, J. N.; Yarmoff, J. A. Site-Specific Neutralization of Low Energy $^{7}Li^{+}$ Scattered from Na/Al(100). *Phys. Rev. Lett.* **1993**, *70*, 3510−3513.

(6) Kimmel, G. A.; Cooper, B. H. Dynamics of Resonant Charge Transfer in Low-Energy Alkali-Metal-Ion Scattering. *Phys. Rev. B* **1993**, *48*, 12164.

(7) Marston, J. B.; Andersson, D. R.; Behringer, E. R.; Cooper, B. H.; DiRubio, C. A.; Kimmel, G. A.; Richardson, C. Many-Body Theory of Charge Transfer in Hyperthermal Atomic Scattering. *Phys. Rev. B* **1993**, *48*, 7809.

(8) Behringer, E. R.; Andersson, D. R.; Cooper, B. H.; Marston, J. B. Charge Transfer in Hyperthermal Energy Collisions of Li^{+} with Alkali-Metal-Covered Cu(001). I. Dynamics of Charge State Formation. *Phys. Rev. B* **1996**, *54*, 14765−14779.

(9) Borisov, A. G.; Teillet-Billy, D.; Gauyacq, J. P.; Winter, H.; Dierkes, G. Resonant Charge Transfer in Grazing Scattering of Alkali-Metal Ions from an Al(111) Surface. *Phys. Rev. B* **1996**, *54*, 17166−17174.

(10) Weare, C. B.; Yarmoff, J. A. Resonant Neutralization of 7li+ Scattered from Alkali/Al(100) as a Probe of the Local Electrostatic Potential. *Surf. Sci.* **1996**, *348*, 359−369.

(11) Borisov, A. G.; Kazansky, A. K.; Gauyacq, J. P. Finite Time Effect in the Charge Transfer Process During an Ion-Metal Surface Collision. *Phys. Rev. Lett.* **1998**, *80*, 1996−1999.

(12) Goryunov, D. G.; Borisov, A. G.; Makhmetov, G. E.; Teillet-Billy, D.; Gauyacq, J. P. Li+ Neutralisation in Back-Scattering from Alkali/Al(100) Surfaces: Comparison between the Various Alkalis. *Surf. Sci.* **1998**, *401*, 206−219.

(13) Borisov, A. G.; Kazansky, A. K.; Gauyacq, J. P. Resonant Charge Transfer in Ion−Metal Surface Collisions: Effect of a Projected Band Gap in the H^{-}-Cu(111) System. *Phys. Rev. B* **1999**, *59*, 10935−10949.

(14) Hecht, T.; Winter, H.; Borisov, A. G.; Gauyacq, J. P.; Kazansky, A. K. Role of 2d Surface State Continuum and Projected Band Gap in Charge Transfer in Front of a Cu(111) Surface. *Phys. Rev. Lett.* **2000**, *84*, 2517.

(15) Yarmoff, J. A.; Yang, Y.; Liu, G. F.; Chen, X.; Sroubek, Z. Charge Exchange in Low-Energy Ion-Surface Scattering. *Vacuum* **2004**, *73*, 25.

(16) Canário, A. R.; Borisov, A. G.; Gauyacq, J. P.; Esaulov, V. A. Nonadiabatic Effects in Atom-Surface Charge Transfer. *Phys. Rev. B* **2005**, *71*, 121401.

(17) Garcia, E. A.; Gonzalez Pascual, C.; Bolcatto, P. G.; Passeggi, M. C. G.; Goldberg, E. C. Ion Fractions in the Scattering of Hydrogen on Different Reconstructed Silicon Surfaces. *Surf. Sci.* **2006**, *600*, 2195.

(18) Wiatrowsky, M.; Lavagnino, N.; Esaulov, V. A. Li+ Ion Neutralization on Ag Layers Grown on Cu(1 1 1). *Surf. Sci. Lett.* **2007**, *601*, L39.

(19) Bonetto, F.; Romero, M. A.; Garcia, E. A.; Vidal, R. A.; Ferrón, J.; Goldberg, E. C. Large Neutral Fractions in Collisions of Li+ with a Highly Oriented Pyrolytic Graphite Surface: Resonant and Auger Mechanisms. *Phys. Rev. B* **2008**, *78*, 075422.

(20) Hamoudi, H.; Dablemont, C.; Esaulov, V. A. Interaction of Li+ with a Au(100) Surface. *Surf. Sci.* **2008**, *302*, 2486.

(21) Garcia, E. A.; Romero, M. A.; Gonzalez Pascual, C.; Goldberg, E. C. Neutralization of Li+ Ions Scattered by the Cu (100) and (111) Surfaces: A Localized Picture of the Atom-Surface Interaction. *Surf. Sci.* **2009**, *603*, 597−605.

(22) Chen, L.; Shen, J.; Jia, J.; Kandasamy, T.; Bobrov, K.; Guillemot, L.; Fuhr, J. D.; Martiarena, M. L.; Esaulov, V. A. Li+-Ion Neutralization on Metal Surfaces and Thin Films. *Phys. Rev. A* **2011**, *84*, 052901.

(23) Vidal, R. A.; Bonetto, F.; Ferrón, J.; Romero, M. A.; Garcia, E. A.; Goldberg, E. C. Electron Captureand Loss in the Scatteringof H+ from Hopg Graphite. *Surf. Sci.* **2011**, *605*, 18.

(24) Meyer, C.; Bonetto, F.; Vidal, R.; García, E. A.; Gonzalez, C.; Ferrón, J.; Goldberg, E. C. Understanding the High Neutralization Yields in Collisions of Kev Li^{+} Ions with Copper Surfaces. *Phys. Rev. A* **2012**, *86*, 032901.

(25) Romero, M. A.; Iglesias-García, A.; Goldberg, E. C. Quantum-Mechanical Interference in Charge Exchange between Hydrogen and Graphene-Like Surfaces. *J. Phys.: Condens. Matter* **2012**, *24*, 045004.

(26) Nordlander, P.; Tully, J. C. Energy Shifts and Broadening of Atomic Levels near Metal Surfaces. *Phys. Rev. B* **1990**, *42*, 5564.

(27) Brongersma, H. H.; Draxler, M.; de Ridder, M.; Bauer, P. Surface Composition Analysis by Low-Energy Ion Scattering. *Surf. Sci. Rep.* **2007**, *62*, 63.

(28) Niedfeldt, K.; Carter, E. A.; Nordlander, P. First Principles Resonance Widths for Li near an Al(001) Surface: Predictions of Scattered Ion Neutralization Probabilities. *J. Chem. Phys.* **2004**, *121*, 3751.

(29) Canario, A. R.; Kravchuk, T.; Esaulov, V. A. Bandgaps, Surface States and the Anomalous Neutralization of Li+ on (111) Surfaces of Noble Metals. *New J. Phys.* **2006**, *8*, 227.

(30) Kravchuk, T.; Bandourine, Y.; Hoffman, A.; Esaulov, V. A. Site Specific Effects in Alloy Surface Reactivity Probed by Li Ions. *Surf. Sci. Lett.* **2006**, *600*, L265−L268.

(31) Niedfeldt, K.; Nordlander, P.; Carter, E. A. Mechanism of Enhanced Broadening of the Ionization Level of Li Outside Transition Metal Surfaces. *Phys. Rev. B* **2006**, *74*, 115109.

(32) Niedfeldt, K.; Carter, E. A.; Nordlander, P. Influence of Surface Band Gaps on the Lifetimes of Charge Transfer States. *Surf. Sci.* **2006**, *600*, L291−L295.
(33) Tamm, I. E. Über Eine Mögliche Art Der Elektronenbindung an Kristalloberflächen. *Z. Physik* **1932**, *76*, 849.
(34) Shockley, W. On the Surface States Associated with a Periodic Potential. *Phys. Rev.* **1939**, *56*, 317−323.
(35) Echenique, P. M.; Pendry, J. B. The Existence and Detection of Rydberg States at Surfaces. *J. Phys. C* **1978**, *11*, 2065.
(36) Borstel, G.; Thörner, G. Inverse Photoemission from Solids: Theoretical Aspects and Applications. *Surf. Sci. Rep.* **1988**, *8*, 1−41.
(37) Smith, N. V. Inverse Photoemission. *Rep. Prog. Phys.* **1988**, *51*, 1227.
(38) Echenique, P. M.; Pendry, J. B. Theory of Image States at Metal Surfaces. *Prog. Surf. Sci.* **1989**, *32*, 111−159.
(39) Johnson, P. D.; Smith, N. V. Image-Potential States and Energy-Loss Satellites in Inverse Photoemission Spectra. *Phys. Rev. B* **1983**, *27*, 2527−2530.
(40) Straub, D.; Himpsel, F. J. Spectroscopy of Image-Potential States with Inverse Photoemission. *Phys. Rev. B* **1986**, *33*, 2256−2262.
(41) Himpsel, F. J.; Ortega, J. E. Electronic Structure of Cu(100), Ag(100), Au(100), and Cu_{3}Au(100) from Inverse Photoemission. *Phys. Rev. B* **1992**, *46*, 9719−9723.
(42) Giesen, K.; Hage, F.; Himpsel, F. J.; Riess, H. J.; Steinmann, W. Two-Photon Photoemission Via Image-Potential States. *Phys. Rev. Lett.* **1985**, *55*, 300−303.
(43) Merry, W. R.; Jordan, R. E.; Padowitz, D. F.; Harris, C. B. Electrons at Metal-Insulator Interfaces: I. The Effect of Xe Monolayers on the Image Potential States of Ag(111). *Surf. Sci.* **1993**, *295*, 393−401.
(44) *Electromagnetic Waves: Recent Development in Research*; Fauster, T., Steinmann, W., Eds.; Elsevier: Amsterdam, 1995; Vol. 2.
(45) Nielsen, H. B.; Brostrom, G.; Matthias, E. Image State Linewidth on Ag(100) Studied by Two-Photon Photoemission Spectroscopy. *Z. Physik* **1989**, *77*, 91.
(46) Steinmann, W. Spectroscopy of Image-Potential States by Two-Photon Photoemission. *Appl. Phys. A* **1989**, *49*, 365.
(47) Höfer, U.; Shumay, I. L.; Reuß, C.; Thomann, U.; Wallauer, W.; Fauster, T. Time-Resolved Coherent Photoelectron Spectroscopy of Quantized Electronic States on Metal Surfaces. *Science* **1997**, *277*, 1480−1482.
(48) Petek, H.; Ogawa, S. Femtosecond Time-Resolved Two-Photon Photoemission Studies of Electron Dynamics in Metals. *Prog. Surf. Sci.* **1997**, *56*, 239−310.
(49) Shumay, I. L.; Höfer, U.; Reuß, C.; Thomann, U.; Wallauer, W.; Fauster, T. Lifetimes of Image-Potential States on Cu(100) and Ag(100) Measured by Femtosecond Time-Resolved Two-Photon Photoemission. *Phys. Rev. B* **1998**, *58*, 13974−13981.
(50) Ueba, H.; Gumhalter, B. Theory of Two-Photon Photoemission Spectroscopy of Surfaces. *Prog. Surf. Sci.* **2007**, *82*, 193−223.
(51) Schoenlein, R. W.; Fujimoto, J. G.; Eesley, G. L.; Capehart, T. W. Femtosecond Studies of Image-Potential Dynamics in Metals. *Phys. Rev. Lett.* **1988**, *61*, 2596−2599.
(52) Lingle, R. L., Jr; Ge, N. H.; Jordan, R. E.; McNeill, J. D.; Harris, C. B. Femtosecond Studies of Electron Tunneling at Metal-Dielectric Interfaces. *Chem. Phys.* **1996**, *205*, 191−203.
(53) Wolf, M.; Knoesel, E.; Hertel, T. Ultrafast Dynamics of Electrons in Image-Potential States on Clean and Xe-Covered Cu(111). *Phys. Rev. B* **1996**, *54*, R5295−R5298.
(54) Schoenlein, R. W.; Fujimoto, J. G.; Eesley, G. L.; Capehart, T. W. Femtosecond Relaxation Dynamics of Image-Potential States. *Phys. Rev. B* **1991**, *43*, 4688−4698.
(55) McNeill, J. D.; Lingle, R. L., Jr.; Ge, N. H.; Wong, C. M.; Jordan, R. E.; Harris, C. B. Dynamics and Spatial Distribution of Electrons in Quantum Wells at Interfaces Determined by Femtosecond Photoemission Spectroscopy. *Phys. Rev. Lett.* **1997**, *79*, 4645−4648.
(56) Chulkov, E. V.; Silkin, V. M.; Echenique, P. M. Image Potential States on Metal Surfaces: Binding Energies and Wave Functions. *Surf. Sci.* **1999**, *437*, 330−352.
(57) Bolcatto, P. G.; Goldberg, E. C.; Passeggi, M. C. G. Interaction between Atoms and Surfaces: A Bond-Pair Description Based on an Extended Anderson Model. *Phys. Rev. B* **1998**, *58*, 5007.
(58) Torralba, M. C.; Bolcatto, P. G.; Goldberg, E. C. Calculation of Ion-Surface Collisions for a Wide Range of Scattering Geometries. *Phys. Rev. B* **2003**, *68*, 075406.
(59) Gross, A. *Theoretical Surface Science: A Microscopic Perspective*, 2nd ed.; Springer-Verlag: Berlin, 2009.
(60) Lewis, J. P.; Glaesemann, K. R.; Voth, G. A.; Fritsch, J.; Demkov, A. A.; Ortega, J.; Sankey, O. F. Further Developments in the Local-Orbital Density-Functional-Theory Tight-Binding Method. *Phys. Rev. B* **2001**, *64*, 195103.
(61) Jelinek, P.; Wang, H.; Lewis, J. P.; Sankey, O. F.; Ortega, J. Multicenter Approach to the Exchange-Correlation Interactions in Ab Initio Tight-Binding Methods. *Phys. Rev. B* **2005**, *71*, 235101.
(62) Smith, N. V.; Chen, C. T.; Weinert, M. Distance of the Image Plane from Metal Surfaces. *Phys. Rev. B* **1989**, *40*, 7565.
(63) Maazouz, M.; Borisov, A. G.; Esaulov, V. A.; Gauyacq, J. P.; Guillemot, L.; Lacombe, S.; Teillet-Billy, D. Effect of Metal Band Characteristics on Resonant Electron Capture: H-Formation in the Scattering of Hydrogen Ions on Mg, Al, and Ag Surfaces. *Phys. Rev. B* **1997**, *55*, 13869−13877.